Title: Fiber photometry does not reflect spiking activity in the striatum

Authors: Alex A. Legaria[1], Julia A. Licholai[2], Alexxai V. Kravitz[1,3,4]

Affiliations:

[1]Department of Neuroscience, Washington University School of Medicine, St Louis, MO
[2]Brown University Department of Neuroscience, Providence, RI
[3]Department of Psychiatry, Washington University School of Medicine, St Louis, MO
[4]Department of Anesthesiology, Washington University School of Medicine, St Louis, MO

Lead contact:
Alexxai V. Kravitz
425 S Euclid Ave, CSRB 5536
Saint Louis, MO 63110
alexxai@email.wustl.edu
(314) 362-5184

Funding: Research funded by the National Institutes of Health Intramural Research Program (NIDDK), Washington University School of Medicine, and NARSAD Young Investigator Grant to AVK.

Keywords: Striatum, calcium imaging, electrophysiology, fiber photometry, spiking

Conflict of interest statement: The authors declare no conflict of interest.

Abstract:

Fiber photometry recordings are commonly used as a proxy for neuronal activity, based on the assumption that increases in bulk calcium fluorescence reflect increases in spiking of the underlying neural population. However, this assumption has not been adequately tested. Here, using endoscopic calcium imaging in the striatum we report that the bulk fluorescence signal correlates weakly with somatic calcium signals, suggesting that this signal does not reflect spiking activity, but may instead reflect subthreshold changes in neuropil calcium. Consistent with this suggestion, the bulk fluorescence photometry signal correlated strongly with neuropil calcium signals extracted from these same endoscopic recordings. We further confirmed that photometry did not reflect striatal spiking activity with simultaneous *in vivo* extracellular electrophysiology and fiber photometry recordings in awake behaving mice. We conclude that the fiber photometry signal should not be considered a proxy for spiking activity in neural populations in the striatum.

Significance statement:

Fiber photometry is a technique for recording brain activity that has gained popularity in recent years due to it being an efficient and robust way to record the activity of genetically defined populations of neurons. However, it remains unclear what cellular events are reflected in the photometry signal. While it is often assumed that the photometry signal reflects changes in spiking of the underlying cell population, this has not been adequately tested. Here, we processed calcium imaging recordings to extract both somatic and non-somatic components of the imaging field, as well as a photometry signal from the whole field. Surprisingly, we found that the photometry signal correlated much more strongly with the non-somatic than the somatic signals. This suggests that the photometry signal most strongly reflects subthreshold changes in calcium, and not spiking. We confirmed this point with simultaneous fiber photometry and extracellular spiking recordings, again finding that photometry signals relate poorly to spiking in the striatum. Our results may change interpretations of studies that use fiber photometry as an index of spiking output of neural populations.

Introduction:

Fiber photometry is a technique for recording bulk calcium emission from genetically identified neuronal populations. However, it remains unclear whether the photometry signal reflects changes in spiking of the underlying population or subthreshold changes in neuropil calcium. To investigate these possibilities, we performed endoscope calcium imaging in the striatum and found that the photometry signal correlated poorly with calcium signals isolated from neuronal cell bodies. Instead, the photometry signal correlated strongly with calcium signals extracted from the neuropil. This suggests that the photometry signal does not reflect changes in spiking of the recorded neuronal populations, but instead may reflect changes in subthreshold calcium. We confirmed this result by simultaneously recording fiber photometry and extracellular spiking, again finding weak relationships between the photometry signal and changes in neuronal spiking. We conclude that the fiber photometry signal should not be considered an index of spiking, as it reflects more strongly changes in neuropil calcium.

Results:

Calcium imaging correlates of fiber photometry

In microscope-based calcium imaging, the potential for neuropil to contaminate somatic calcium signals has been noted for more than a decade and has motivated both optical and analytical approaches to isolate somatic calcium signals from neuropil (1–4). However, these approaches cannot be applied to fiber photometry as the technique does not focus the excitation light nor retain spatial information of emitted fluorescence. Therefore fiber photometry can collect fluorescence from both somatic and non-somatic (neuropil) sources (figure 1A). To investigate how each of these sources contributes to the fiber photometry signal, GCaMP6s was expressed in the dorsal striatum of 6 mice using a viral strategy that transduced all striatal neurons non-selectively. In the same surgery, a graded index (GRIN) lens was implanted above the viral expression zone, and a steel head bar was attached for head fixation. Calcium imaging was performed using a fluorescent endoscopic microscope in head-fixed mice (Mightex OASIS Implant, figure 1B). Somatic calcium activity was extracted from these recordings using the CaImAn python package (5) which implements a constrained non-negative matrix factorization for micro-endoscopic data (CNMF-E) algorithm (2). We selected the 10 highest quality somatic signals from each recording, assessed by isolation metrics and manual inspection of the extracted signal. We also extracted 10 regions of interest (ROIs) that were devoid of cell bodies for analysis of neuropil signals from these same recordings (figure 1C). Finally, we extracted the fluorescence intensity of the whole field (WF), which we termed the photometry signal (figure 1D).

The photometry signal correlated surprisingly weakly with somatic signals (average R = 0.21), which also correlated weakly with each other (range of R values: -0.04 to 0.34, figure 1E, G). In contrast, the photometry signal correlated strongly with all extracted neuropil ROIs (average R = 0.92, figure 1F, G), which also correlated strongly with one another (range of R values: 0.88 to 0.96, figure 1F, G). Overall, less than 5% of the variance in the fiber photometry signal was explained by somatic calcium signals, while more than 84% was explained by neuropil calcium signals.

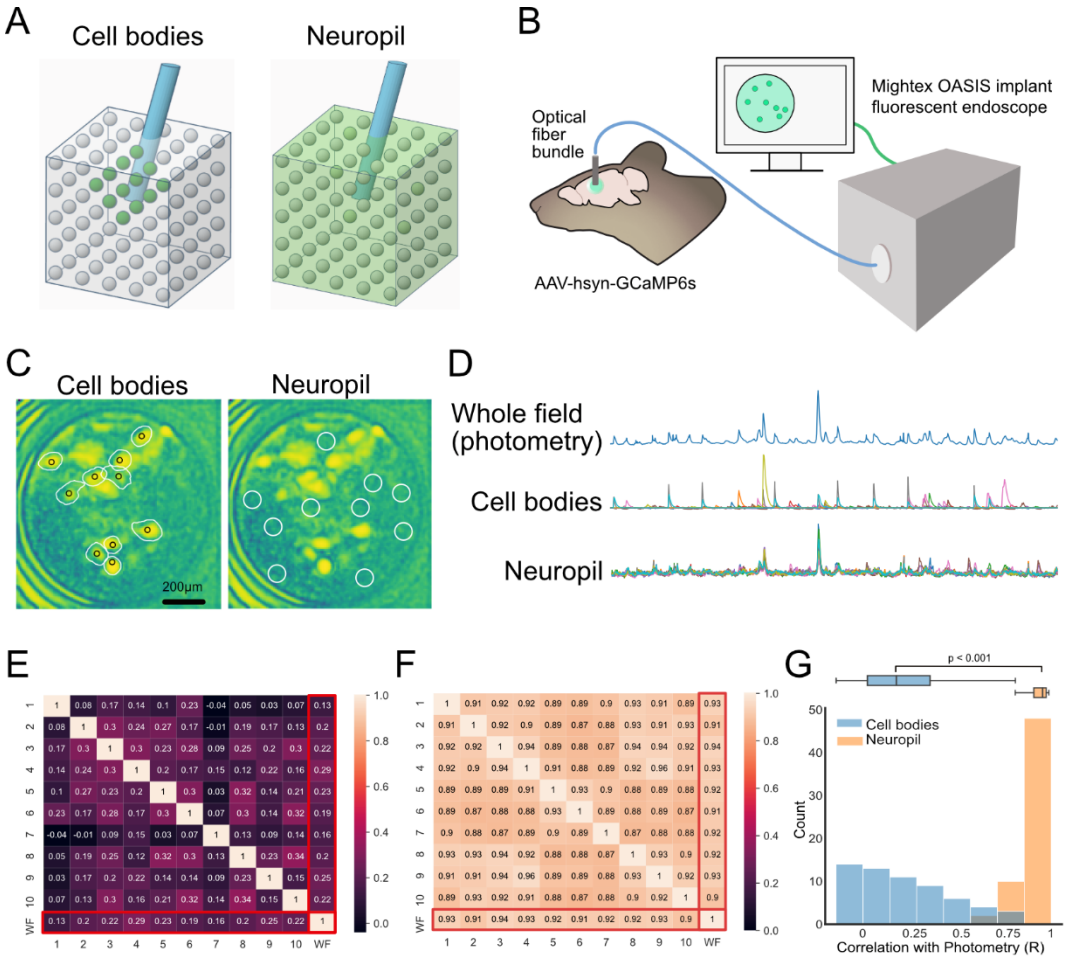

Figure 1. Fiber photometry signals correlate with neuropil but not cell body calcium. (A) Schematic of how somatic (Left) or neuropil (Right) fluorescence can contribute to fiber photometry signal. **(B)** Experimental setup of endoscopic GRIN lens recordings in striatum of awake head fixed mice. **(C)** Images of maximal projection image through GRIN lens showing extracted cell body signals (Left, using CaImAn for cell body isolation), or neuropil regions of interest (ROIs, Right). **(D)** Example traces of a whole-field photometry signal (top), cell body signals (middle), or neuropil signals (bottom) extracted from the same recording. **(E)** Correlation matrix for ten cell body signals and the whole field (WF) photometry signal **(F)** Correlation matrix for ten neuropil signals and the whole field (WF) photometry signal. **(G)** Histogram of correlation coefficients (R) between photometry signal and cell bodies or neuropil. Statistical analysis: Welch's T-test.

Electrophysiological correlates of fiber photometry.

To test our finding with an alternative approach, we performed simultaneous fiber photometry and electrophysiological recordings in awake freely moving awake mice (n=5). We expressed GCaMP6s in the ventral striatum using either a non-specific viral strategy in wildtype mice (n=3) or a cre-dependent strategy in Drd1-cre mice (n=2). In the same surgery, we implanted an array of 32 tungsten microwires surrounding an optical fiber for collecting photometry signals (figure 2A, B). Photometry signals were recorded and digitized simultaneously with multiunit spiking (figure 2A) for 60-120 minutes, resulting in spiking from 50 multiunits and 17 single units (average of 13.4 units per mouse).

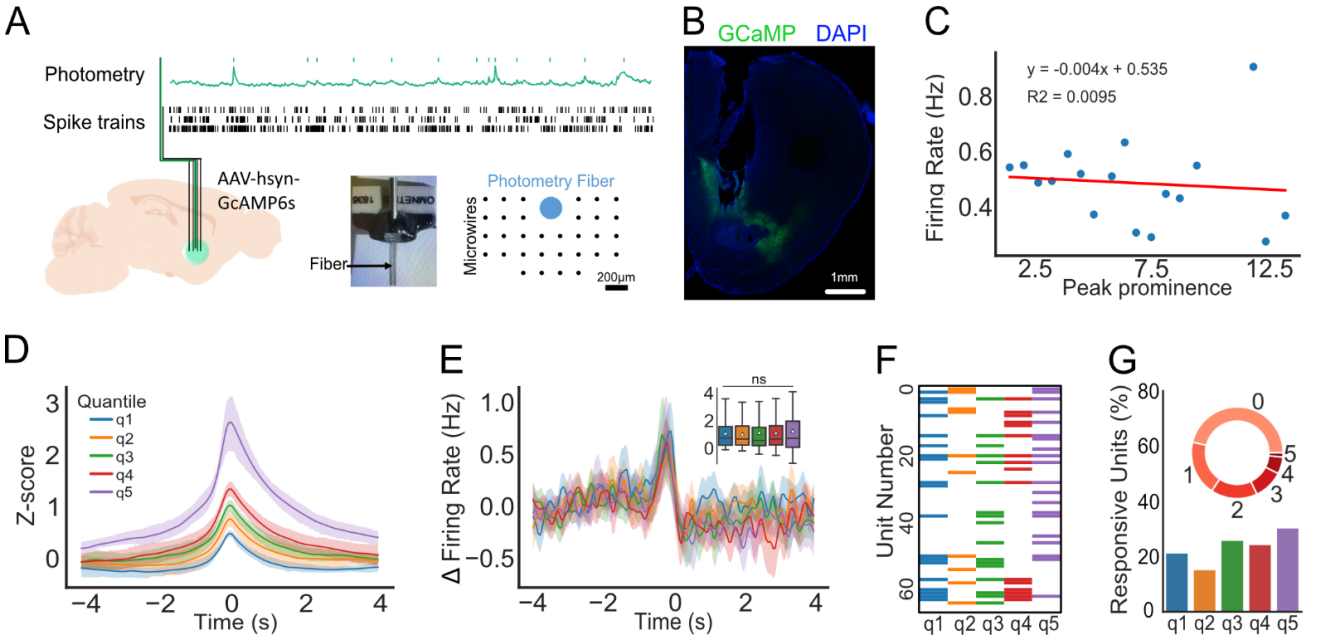

Figure 2. Photometry transient size does not relate to amount of neuronal spiking. (A) Experimental setup: An optical fiber coupled to a 32-channel array (lower right) was implanted in the ventral striatum to simultaneously record fiber photometry signals and multiunit spiking. **(B)** Photograph showing fiber/array implantation and GCaMP expression in ventral striatum. **(C)** Correlation between calcium transient size and firing rate of all recorded units. **(D)** Average calcium fluorescence split into five equal quantiles of calcium transient size (q1 - q5). **(E)** Average change in multiunit firing rate aligned to each quantile. Inset: Average change in firing of each quantile. **(F)** Heat map of units that increased spiking to each of the quantiles. Colored boxes indicate that the unit showed increased spiking around photometry transient **(G)** Percent of units that increased spiking to each of the quantiles. Inset: Number of neurons that were responsive to displayed number of the quantiles.

We observed fluctuations in calcium with a fast rise and slow decay which we termed “photometry transients” (6–9), which were of variable size (figure 2A). We asked whether the amplitude of photometry transients correlated with average firing rate in a 1s window around each transient, but found no relationship between these variables (figure 2C). In other words, larger photometry transients were not associated with greater firing rates in the underlying tissue. Next, we asked whether the magnitude of photometry transients correlated with the *change* in striatal firing. To test this, we divided the transients into 5 quantiles based on their peak prominence (figure 2D), but again observed no relationship between the amplitude of photometry transients and magnitude of change in striatal spiking

(figure 2E). Finally, we considered if larger photometry transients might reflect an increased *number* of activated neurons, independent of the levels of spiking in these neurons. Here, we counted the number of neurons that exhibited significant changes in spiking around the photometry transients in each quantile (figure 2F). Again, larger photometry transients were not associated with larger numbers of responsive neurons (figure 2G). We conclude that the amplitude of photometry transients is not related to the amount nor change in striatal spiking activity.

Discussion:

Based on these experiments, photometry recordings in the striatum do not appear to reflect changes in somatic calcium nor neuronal spiking. Instead, these signals correlate most strongly with calcium signals extracted from the neuropil. This finding is consistent with one study that previously reported correlations between simultaneously recorded spiking and photometry, where spiking explained a small amount of the variance (~10% based on reported R values) in the photometry signal (10). Our finding is also not surprising, as neuropil calcium is known to influence calcium signals in microscope-based imaging (1–4). Recently, new approaches have limited the expression of GCaMP to the soma to mitigate the contribution of neuropil in calcium imaging (11, 12). Despite knowledge of this issue and the widespread use of fiber photometry, there have been few attempts to quantify the relative contribution of neuropil vs. spiking to the fiber photometry signal. Here, we demonstrate that the fiber photometry signal in the striatum relates weakly to somatic calcium and spiking, and strongly to neuropil calcium. Due to the large dendritic arbors of striatal neurons (13), the majority of the neuropil signal is likely dendritic and may therefore reflect inputs to the striatum, rather than outputs from the striatum.

There are also some limitations to our study. First, the results presented here are limited to recordings in the striatum. Striatal neurons have extensive dendritic arbors, which may accentuate the neuropil contribution to the fiber photometry signal. Fiber photometry signals from other brain structures may result in different conclusions concerning the relative contributions of somatic versus neuropil calcium. Second, our recordings were performed with GCaMP6s, a variant of GCaMP that has slow dynamics. Different relationships may be observed with GCaMP variants with faster kinetics, or those that target GCaMP to specific cellular compartments (11, 12). Despite these limitations, we believe our results speak to the utility of fiber photometry, and the interpretation of findings with this technique. We conclude that fiber photometry should not be interpreted as a representation of spiking activity of the fluorescence neurons being recorded, but rather the *total* calcium signal of these cells, including both subthreshold changes in dendritic activity as well as changes in neuronal spiking.

Acknowledgements: We thank the GENIE project at Janelia Research Campus for their generous development and sharing of GCaMP reagents. We thank the NIH Section on Instrumentation for designing and building the head-fixed wheel apparatus for calcium imaging.

Author Contributions: Alex Legaria: Methodology, Investigation, Formal analysis, Writing, Review & Editing; **Julia Licholai**: Methodology, Investigation; **Alexxai V. Kravitz**: Methodology, Writing, Review & Editing, Supervision, Funding acquisition

Methods:

Subjects:

The animals used in this study were 9 wild-type C57BL6 mice and 2 Drd1-Cre mice on a C57BL6 background. Animals were housed at either the National Institutes of Health (NIH) or Washington University in St Louis animal facilities in standard vivarium cages with *ad libitum* food and water and 12-hour dark/light cycle. All experimental procedures were approved by the National Institute of Diabetes and Digestive and Kidney Diseases (NIDDK) Animal Care and Use Committee and the Washington University Animal Care and Use Committee.

Viral transduction:

Anesthesia was induced with isoflurane at 3-5% and maintained at 0.5-1.5% during the surgery delivered via a mouse mask mounted on a stereotaxic apparatus. Ear bars and mouth holder were used to keep the mouse head in place while the skin was shaved and disinfected with a povidone/iodine solution. The skull was exposed and 1.0mm diameter hole was performed with a microdrill that was mounted on the stereotaxic frame. Injections were performed with either a 33 gauge steel injector (Plastics1) using a hydraulic infusion system connected to a syringe pump (World Precision Instruments) or a glass pipette mounted in a Nanoject 3 infusion system (Drummond Scientific). For both systems, 500nL of virus AAV1-Syn-GCaMP6s (UPenn Vector Core) virus was infused over 10 minutes into either the dorsal striatum (AP +0.5 mm, ML +1.5 mm, DV -2.8 mm) or ventral striatum (AP +0.5 mm, ML +1.2 mm, DV -4.5 mm). The injector was left in place for 5 minutes after surgery before removal.

Gradient Index (GRIN) lens and head bar implantation:

Following viral infusion, a GRIN lens (Inscopix GLP-0560, 0.5mm in diameter, 6.1 mm long) was implanted into 6 mice in the same surgery. The lens was mounted on the stereotaxic frame with a custom holder, and slowly lowered into the same tract as the virus without aspirating or mechanically removing any additional tissue. When the lens reached 2.6mm below the surface of the skull it was cemented in place with C&B Metabond® Quick Adhesive Cement System and the implant was fortified with black acrylic dental cement (Lang Dental). Finally, a custom stainless steel head-bar was placed on the top of the implant and secured with additional acrylic dental cement. After the cement fully cured animals were placed back in their home-cage on a pre-heated pad at 37°C. After full recovery, animals received a subcutaneous injection of buprenorphine (0.05 mg/kg) and were returned to their home-cages for recovery. Animals recovered for at least 4 weeks before recording to enable time for the inflammatory response around the GRIN lens to subside.

Implantation of electrode array:

Following viral infusion, a combined electrophysiology/fiber photometry device was implanted into 5 mice. Here, fiber optic cannulae (200 µm, 0.50 NA) with 1.25mm ceramic ferrules were purchased from Thorlabs and cut to 6mm. These cannulae were mounted in a custom electrode array with 32 Teflon-coated tungsten microwires (35 µm diameter; Innovative Neurophysiology) that surrounded a central gap where the photometry fiber was mounted. This combined photometry/electrical recording device was implanted into the right DMS (AP, +0.5 mm, ML, +1.5 mm, DV, -2.8 mm). The device was secured to skull with a thin layer of adhesive dental cement (C &B Metabond, Parkell) followed by a larger layer of acrylic dental dement (Lang Dental). After the cement fully cured animals were placed back in their home-cage on a pre-heated pad at 37°C. After recovery, animals received a subcutaneous injection of meloxicam (10 mg/Kg) and were returned to their home-cages for recovery. Mice recovered for at least 2 weeks to allow for viral expression prior to recording.

Calcium imaging recordings:

Mice were habituated to head-fixation over a period of 2-3 weeks. This started with brief (1-2 minute) sessions of head-fixation, expanding to 30-60 minutes with daily sessions over 2-3 weeks. The head-

fixation took place on a custom wheel (8" in diameter) mounted in an aluminum frame with bilateral steel head fixation bars (NIH Section on Instrumentation). After mice tolerated head fixation for 30 minutes we commenced with calcium imaging recordings. An endoscopic epifluorescence microscope (Mightex OASIS Implant) was used for these recordings. This microscope was equipped with a Lumencor Aura fluorescence light engine to delivered 475nm light to the GRIN lens, a fluorescence filter set for imaging green GCaMP fluorescence, and a PCO Edge camera for capturing images. The excitation and emission light was transmitted through a 600micron or 350micron flexible fiber bundle to the GRIN lens for collection of calcium imaging data. The microscope and data acquisition was controlled with NIS Elements software (Nikon). Image pre-processing was also performed in NIS Elements and included background subtraction and de-noising. Videos of cellular activity were between 846 and 2999 frames in length.

Calcium imaging processing:

Somatic activity extraction. We used the CaImAn cell body extraction Jupyter notebook pipeline (5) to identify somatic activity. Briefly, this pipeline implements motion correction and the CNMF-E algorithm (2) in an online notebook, returning quality metrics and images of extracted somatic signals for subsequent analysis. From each movie, we selected 10 somatic signals for further analysis based on returned quality metrics and a qualitative assessment.

Neuropil activity extraction. Neuropil signals were extracted using the FIJI distribution of ImageJ (14). We performed a maximum projection across time to identify areas of the image with no obvious somatic calcium. We placed 10 regions-of-interest (ROIs) on each movie, sampling a wide range of the spatial area while avoiding somatic signals, and extracted the signals from each across time. The size of the ROIs was the average size of identified somatic calcium signals.

Extraction of photometry signals. Photometry signals used in figure 1D-H were extracted from Image J by placing a single ROI covering the entire spatial area of the lens and extracting the signal across time.

Electrophysiology and fiber photometry acquisition:

Neurophysiological signals were recorded by a multi-channel neurophysiology system (Omniplex, Plexon Inc). Spike channels were acquired at 40 kHz and band-pass filtered at 150 Hz to 3 kHz before spike sorting. Fiber photometry acquisition was performed with a Neurophotometrics fiber photometry system, with fluorescence output data processed in Bonsai (https://bonsai-rx.org/docs) and transmitted in real-time as a voltage signal that was acquired by the Plexon Omniplex.

Electrophysiology/Fiber photometry data analysis:

Single and multiunits were manually discriminated using principal component analysis (Offline Sorter; Plexon), using MANCOVA analyses to determine if single unit clusters were statistically distinct from multi-unit clusters. Where single unit isolation did not reach statistical significance, spike clusters were combined into multiunits. Data analysis was performed using a custom Python/Neuroexplorer pipeline (code available at: https://osf.io/8j7g2/), described below.

Photometry signal preprocessing. The fiber photometry signal was processed using a custom python/Neuroexplorer5 pipeline (code available at: https://osf.io/8j7g2/). We first applied both a lowpass (6Hz) and a highpass filter (0.0005Hz) to the photometry signal to correct for high frequency noise and photo bleaching, respectively. Photometry peaks were then identified using the scipy.signal.find_peaks function, setting a prominence threshold of 1. Photometry peak amplitude quantiles were created by diving the peak timestamps into five groups containing an equal number of peaks each, using the pandas function pd.qcut.

Classification of responsive units. The classification of responsive units in Figure 2 F-G was done by creating a peri-event histogram (PEH) of each neuron using each photometry peak quantiles as a

reference (figure 2D). To assess the change in firing rate we set a baseline period for each neuron (-4 to -2 seconds from the photometry peak) and subtracted its average from the entire PEH signal. A neuron was considered responsive if the signal window (-1 to 1 seconds from the photometry peak) was at least 3 standard deviations higher than the average of the baseline window for at least 250 consecutive milliseconds. We chose 3 standard deviations based on a permutation analysis that demonstrated <1% false positives with this threshold.

Histology:

At the end of the experiments we performed histological verification of implant placements. Animals were anesthetized with isoflurane, decapitated, and their brains were quickly removed and placed in 10% formalin solution. Brains were incubated overnight in 10% formalin solution, and then moved to 30% sucrose solution until sectioning. Coronal slices containing the striatum were prepared using a freezing microtome (Leica SM2010R). Slices were mounted on microscope slides with a mounting media and imaged with an epifluorescence microscope (Zeiss). For in vivo electrophysiology electrode placement was assessed via observation of implant tract or electric-lesions that were made under anesthesia before decapitation (performed with a 5-s long pulse of 10 mA; Ugo Basile Lesion Making Device).

Data and code availability: All data and code are available here: https://osf.io/8j7g2/).

References

1. S. W. Keemink, *et al.*, FISSA: A neuropil decontamination toolbox for calcium imaging signals. *Scientific Reports* **8**, 3493 (2018).

2. E. A. Pnevmatikakis, *et al.*, Simultaneous Denoising, Deconvolution, and Demixing of Calcium Imaging Data. *Neuron* **89**, 285–299 (2016).

3. P. Zhou, *et al.*, Efficient and accurate extraction of in vivo calcium signals from microendoscopic video data. *eLife* **7**, e28728 (2018).

4. E. A. Mukamel, A. Nimmerjahn, M. J. Schnitzer, Automated analysis of cellular signals from large-scale calcium imaging data. *Neuron* **63**, 747–760 (2009).

5. A. Giovannucci, *et al.*, CaImAn an open source tool for scalable calcium imaging data analysis. *eLife* **8**, e38173 (2019).

6. G. Cui, *et al.*, Concurrent activation of striatal direct and indirect pathways during action initiation. *Nature* **494**, 238–242 (2013).

7. E. S. Calipari, *et al.*, In vivo imaging identifies temporal signature of D1 and D2 medium spiny neurons in cocaine reward. *Proc Natl Acad Sci U S A* **113**, 2726–2731 (2016).

8. S. Bariselli, N. L. Miyazaki, M. C. Creed, A. V. Kravitz, Orbitofrontal-striatal potentiation underlies cocaine-induced hyperactivity. *Nat Commun* **11**, 3996 (2020).

9. C. Meng, *et al.*, Spectrally Resolved Fiber Photometry for Multi-component Analysis of Brain Circuits. *Neuron* **98**, 707-717.e4 (2018).

10. J. E. Markowitz, *et al.*, The Striatum Organizes 3D Behavior via Moment-to-Moment Action Selection. *Cell* **174**, 44-58.e17 (2018).

11. Y. Chen, *et al.*, Soma-Targeted Imaging of Neural Circuits by Ribosome Tethering. *Neuron* **107**, 454-469.e6 (2020).

12. O. A. Shemesh, *et al.*, Precision Calcium Imaging of Dense Neural Populations via a Cell-Body-Targeted Calcium Indicator. *Neuron* **107**, 470-486.e11 (2020).

13. R. J. Preston, G. A. Bishop, S. T. Kitai, Medium spiny neuron projection from the rat striatum: An intracellular horseradish peroxidase study. *Brain Research* **183**, 253–263 (1980).

14. J. Schindelin, *et al.*, Fiji: an open-source platform for biological-image analysis. *Nature Methods* **9**, 676–682 (2012).